


## Suppression of the wake steady asymmetry of an Ahmed body by central base bleed

Tauha Irfan Khan  and Vladimir Parezanović \*

*Khalifa University of Science and Technology, P.O. Box 127788, Abu Dhabi, United Arab Emirates*

Luc Pastur 

*ENSTA-Paris, Institut Polytechnique de Paris, 828 Bd des Maréchaux, F-91120 Palaiseau, France*

Olivier Cadot 

*School of Engineering, University of Liverpool, Liverpool L69 3GH, United Kingdom*



(Received 4 May 2022; accepted 2 August 2022; published 19 August 2022)

Base blowing is applied through a small, centrally located square aperture at the base of a flat-backed Ahmed body. In addition to the expected drag reduction effect at low momentum injection (i.e., base bleeding effect), a major result is the complete suppression of the steady asymmetry of the wake. Both the maximum drag reduction and the minimum magnitude of the base pressure gradient are achieved for the same optimal blowing coefficient of the actuator. Independent force measurements corroborate the suppression of the wake asymmetry. Different scales of base blowing reveal a similar maximum drag reduction and asymmetry suppression, where the optimal blowing coefficient is found to scale with the bleed-to-base area ratio as  $(S_j/S)^{1/2}$ .

DOI: [10.1103/PhysRevFluids.7.083902](https://doi.org/10.1103/PhysRevFluids.7.083902)

### I. INTRODUCTION

The passive or active injection of fluid into the wake of a bluff body, commonly referred to as base bleed, is a well-known method of drag reduction. It has been widely used for both two-dimensional cylinders [1–3] and three-dimensional axisymmetric bodies [4–8]. More recently, base bleed has been examined in the case of square-back models as active base blowing [9–11], passive ventilation [12], and at industrial scales [13].

On the other hand, the turbulent wake of the flat-backed Ahmed body is dominated by the reflectional symmetry breaking (RSB) mode [14] which causes the wake to switch chaotically between two stable, asymmetric states. This steady wake asymmetry, resulting from a pitchfork bifurcation [15], produces side forces and an increase in drag. The asymmetry can be mitigated by placing a small control cylinder in the wake, which can result in a drag reduction of around 4% [16,17]. Thus, recent efforts have been directed towards the symmetrization of the wake, in order to remove the drag associated with the RSB mode. However, suppressing the RSB mode in the horizontal direction ( $y$  instability) may lead to a permanent wake asymmetry in the vertical direction ( $z$  instability) [10,18–20].

The two cases in which the RSB mode has been completely suppressed in both directions use a rear cavity [21] and a perimetric base suction [22]. In the former case, drag has been reduced and base pressure fluctuations significantly damped, while in the latter base suction increased the overall

---

\*vladimir.parezanovic@ku.ac.ae

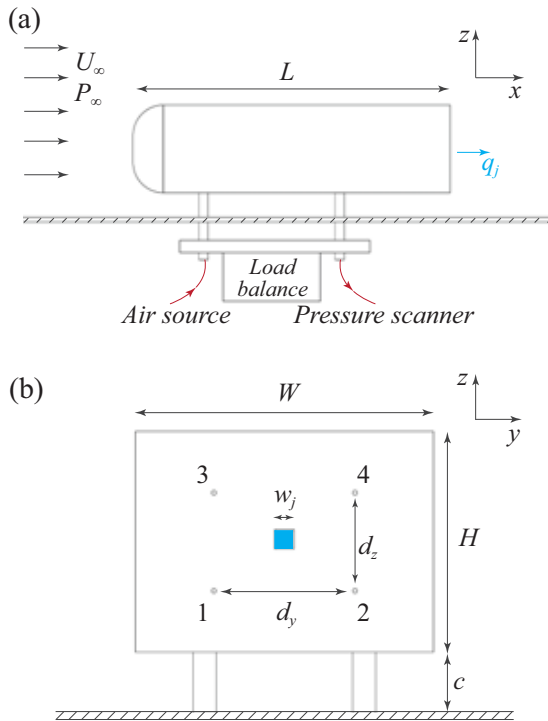


FIG. 1. (a) Side and (b) rear views of the experimental model.

drag, since the recirculation region shrinks due to mass extraction, but also achieved a symmetric wake in both vertical and horizontal directions. In the case of peripheral base blowing [10], the actuation has almost no authority on the steady asymmetry while low drag is observed. More recently, Ref. [23] used a large-scale sweeping jet actuator blowing from the middle of the Ahmed body base. They observed a significant reduction of the steady asymmetry in the wake, although not corresponding to a minimum drag. This result indicated that a centrally located base blowing might be much more effective at symmetrizing the wake than blowing near the shear layers. Inspired by the latter work, we present the results on the drag reduction and suppression of the steady wake asymmetry by a steady jet blowing from the center of the flat-backed Ahmed body base. The effect of scaling for such a type of base blowing is also presented.

## II. EXPERIMENTAL SETUP

The experiments were performed in an Eiffel-type wind tunnel with a test section of  $390 \times 400 \times 1200$  mm ( $h \times w \times l$ ). The square-back bluff body, shown in Fig. 1, has dimensions of  $H = 72$  mm,  $W = 97.25$  mm, and  $L = 261$  mm. The model is mounted above the test section floor keeping a ground clearance of  $c = 20$  mm. Four cylindrical support struts of 7.5 mm diameter are used to mount the model on a platform which is then attached to the load balance. These hollow struts provide access for the air supply for the actuator and the vinyl tubes between the pressure ports and the pressure scanner (which is located below the test section floor). The free stream velocity was maintained at  $U_\infty = 13.5$  m/s which corresponds to  $Re = U_\infty H / \nu \approx 65\,000$ , where  $\nu$  is the kinematic viscosity.

The actuation is performed by a centrally located, steady jet at the base, as shown in Fig. 1. The jet is expelled through a simple square cross-section duct of side ( $w_j$ ), with the bleed-to-base area ratio of  $S_j/S = w_j^2/HW = 0.0057$ . The mass flow rate through the actuator is set using an ALICAT

2000 SLPM flow controller. The flow rate is represented by a dimensionless blowing coefficient  $C_q = q_j/U_\infty HW$ , where  $q_j$  is the volumetric flow rate supplied to the actuator.

Instantaneous pressure at the base of the bluff body  $p_i(t)$  is measured through four static pressure ports, where  $i \in 1, 2, 3, 4$  correspond to labels in Fig. 1(b). The ports are connected via flexible vinyl tubes to a Scanivalve ZOC 22B/32Px pressure scanner, and the pressure is acquired at a rate of 200 Hz over a period of  $T = 30$  s. The instantaneous pressure is presented as a nondimensional pressure coefficient  $c_{p(i)} = [p_i(t) - P_\infty]/q_\infty$ , where  $P_\infty$  and  $q_\infty = \frac{1}{2}\rho U_\infty^2$  are the mean reference static and dynamic pressures of the test section obtained through a Pitot-static tube located upstream and away from the model. The contribution of the base to the pressure drag is expressed as a mean base suction coefficient, averaged over the four pressure ports,

$$C_B = -\frac{1}{4} \sum_{i=1}^4 C_{p(i)}, \quad (1)$$

where  $C_{p(i)} = \langle c_{p(i)} \rangle_T$  is the time-averaged value.

Instantaneous base pressure gradients in the horizontal and vertical direction are calculated as

$$g_y = \frac{c_{p(4)} - c_{p(3)} + c_{p(2)} - c_{p(1)}}{2d_y/H} \quad (2)$$

and

$$g_z = \frac{c_{p(3)} - c_{p(1)} + c_{p(4)} - c_{p(2)}}{2d_z/H}, \quad (3)$$

respectively, where  $d_y = 46$  mm and  $d_z = 32$  mm are the separation distances between the pressure ports. The magnitude of the resulting pressure gradient is defined as  $G = \langle \sqrt{g_y^2 + g_z^2} \rangle_T$  and represents the time-averaged strength of the wake asymmetry.

Force measurements are performed simultaneously with pressure measurements, using a multi-axis load balance AMTI MC3A-500 at an acquisition rate of 1000 Hz and a period of  $T = 30$  s. The measurements of forces are first performed with the model installed and wind tunnel switched off ( $U_\infty = 0$ ), to characterize the contributions of actuation to the forces applied on the bluff body  $f_{(q)k}$  ( $k \in x, y, z$ ), for different  $C_q$ . The wind tunnel is then activated and, after a settling period, the measurements are obtained for the working velocity  $U_\infty$  and varying  $C_q$ . The instantaneous dimensionless force coefficients are then estimated as  $c_k = (f_k - f_{(q)k})/(q_\infty HW)$ , and the corresponding mean quantities are denoted as  $C_k = \langle c_k \rangle_T$ . Finally, the deviation of aerodynamic force coefficients with respect to  $C_q$  is defined as

$$\Delta c_k = c_k(C_q) - C_k(C_q = 0), \quad (4)$$

where  $c_k(C_q)$  is the instantaneous force coefficient for any given  $C_q$ , and  $C_k(C_q = 0)$  is the mean force coefficient for the unactuated flow.

Reference measurements for  $U_\infty$  and  $C_q = 0$  are taken at the beginning and the end of each set of experiments, and are used to correct the pressure and force data for drift. According to the manufacturer specifications for the respective measurement systems, the precision of the instantaneous pressure and force data in terms of dimensionless coefficients is  $\delta(c_p) = \pm 0.04$ ,  $\delta(c_x, c_y) = \pm 0.02$ , and  $\delta(c_z) = \pm 0.075$ . However, the mean values of  $C_B$  and  $C_x$  satisfactorily converge after about 20 s of data, and the standard deviation of their averages over longer times (up to  $T = 30$  s) are less than 0.11% and 0.24% of the mean values, respectively.

### III. RESULTS

The global effects of base blowing for different  $C_q$  are encapsulated in Fig. 2. For the unactuated flow, the absolute values of base suction and drag coefficients are  $C_{B0} = 0.185$  and  $C_{x0} = 0.375$ , respectively. The unactuated values are comparable to data from a similar experiment in Ref. [10]. As

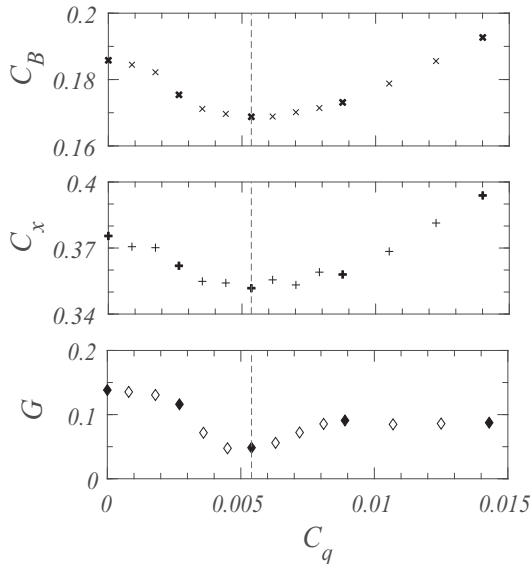


FIG. 2. Evolution of base suction ( $C_B$ ), drag ( $C_x$ ), and wake asymmetry strength ( $G$ ) with respect to the blowing coefficient  $C_q$ . Dashed vertical lines correspond to  $C_q^{\text{opt}}$ . Highlighted points (solid markers) correspond to data points used in Fig. 3.

the blowing coefficient is increased, these values gradually decrease to a minimum at  $C_q^{\text{opt}} = 0.0054$ , where the base suction and drag coefficients are decreased by around 9% and 6%, respectively. For blowing coefficients  $C_q > C_q^{\text{opt}}$  both quantities slowly increase and eventually show a net drag increase for  $C_q > 0.012$ . This behavior is observed also in the experiment of Ref. [10] and is discussed there in the context of the model of the recirculation region length by Ref. [24]. We hypothesize that in the current experiment the flow regime up to  $C_q^{\text{opt}}$  is similar to the “mass” regime, and beyond that value to the “momentum” regime, as proposed by Ref. [10]. However, the mass regime observed in Ref. [10] is characterized by an affine decrease of the drag until the minimum drag is reached. It is modeled by an affine increase of the recirculation length as a consequence of a passive mass injection (i.e., where the momentum of the injected mass is negligible), thus changing globally the recirculating volume. Here, the behavior observed in Fig. 2 becomes nonlinear much before the minimum drag is reached. One then suspects whether the interaction of the blowing jet with the feedback recirculating flow almost centered at the base contributes to extra drag reduction by, for instance, suppressing the RSB mode. As the injection in Ref. [10] is at the periphery of the base, it might miss this beneficial momentum effect. It can be observed that the slopes of  $C_B$  and  $C_x$  start to noticeably diverge from each other at high blowing rates ( $C_q \gg C_q^{\text{opt}}$ ), which indicates that the base suction is no longer accurately estimated using the assumption of a uniform distribution of pressure at the base, due to the intense low-pressure region created by the blowing jet.

The strength of the steady asymmetry in the wake is also represented in Fig. 2, by the modulus of the base pressure gradient  $G$ . The high magnitude of  $G$  for  $0 \leq C_q < 0.027$  indicates a strong asymmetry of the wake for unactuated flow and low actuator mass flow rate cases. The modulus of the pressure gradient is significantly reduced at  $C_q^{\text{opt}}$ , coinciding with the strongest reductions of base suction and drag. At higher blowing coefficients, the wake asymmetry again starts to increase but does not achieve the levels of the unactuated wake.

The presence of the wake RSB mode and its evolution, versus select  $C_q$ , are visualized by the probability density function (PDF) of the pressure gradient  $\mathbf{g}$  in Fig. 3(a). The RSB mode in the horizontal direction is clearly visible for the baseline flow case ( $C_q = 0$ ), where  $g_y$  can have a positive ( $P$  state) or a negative value ( $N$  state) with an almost equal probability. As the flow rate is

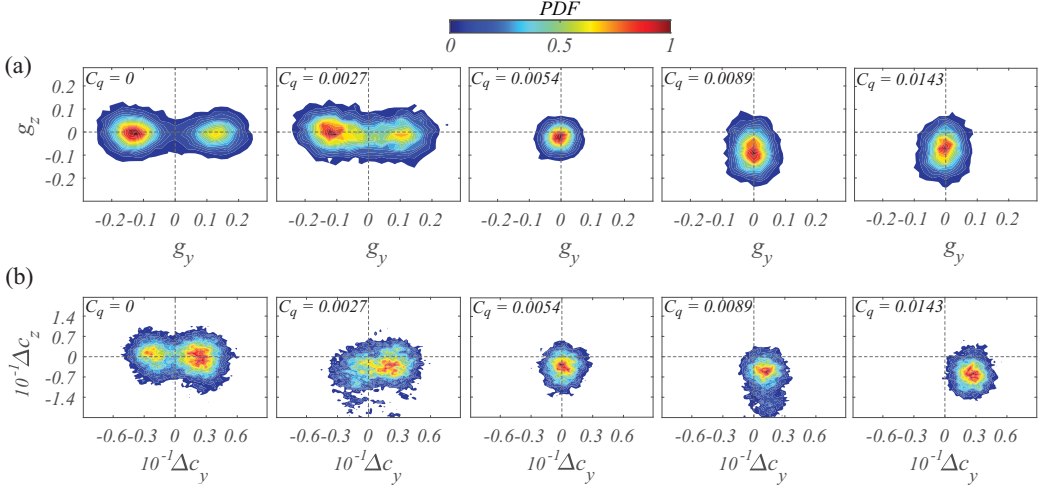


FIG. 3. The joint PDFs of (a) horizontal ( $g_y$ ) and vertical ( $g_z$ ) pressure gradients at the base, and (b) deviations of side force ( $\Delta c_y$ ) and normal force ( $\Delta c_z$ ) coefficients. The color bar represents a normalized PDF with values below 0.004 as white.

increased to  $C_q = 0.0027$ , mode switching between the two asymmetric flow states becomes more frequent, significantly populating the  $g_y = 0$  bin, but high values of  $g_y$  are still highly probable. For  $C_q^{\text{opt}} = 0.0054$  the pressure gradient reduces to a compact, circular distribution centered around zero. This suggests the RSB mode has been suppressed in both horizontal and vertical directions. For higher  $C_q$  the vertical pressure gradient  $g_z$  adopts a steady  $N$  state, indicating that the wake has been vectorized downwards by the base blowing.

The changes to the wake RSB mode are corroborated by the PDF of the deviations of side force and lift force coefficients, in Fig. 3(b). Almost identical patterns of PDFs between the pressure and the forces can be observed, up to and including  $C_q^{\text{opt}}$ . For  $C_q \geq 0.0089$ , the pressure indicates increased fluctuations around a weak  $N$  state of  $g_z$ , which is reflected in the PDF of the lift force. However, the PDF of  $\Delta c_y$  indicates a progressive increase of the mean side force with the increase of  $C_q$  which is not observed by the pressure. Nevertheless, it is clear that at  $C_q^{\text{opt}}$  the fluctuating forces acting on the body are strongly suppressed and comparable in both horizontal and vertical directions. The force measurements confirm that the beneficial effects of the steady jet seen in the pressure gradient are not due to any unwanted interaction between the jet and the pressure measurements at the base, but that the wake is truly more steady and symmetric.

The effect of scaling for this type of flow actuation is also studied. Base blowing is carried out from a similar location using two scaled down actuators. In what follows, the baseline actuator is referred to as  $\times 1$  whereas the scaled down actuators  $\times 0.5$  and  $\times 0.35$  represent scaling with respect to the actuator side  $w_j$ . Figure 4(a) shows the changes in base suction, defined as  $\Delta C_B = C_B - C_{B0}$ , for all scales of actuators. We observe that the scaled down actuators  $\times 0.5$  and  $\times 0.35$  achieve a similar base suction reduction as the  $\times 1$  actuator, however, the maximum drag reduction is achieved at a lower  $C_q^{\text{opt}} = 0.0027$  and  $0.0018$ , respectively. The result from the experiment conducted by Ref. [11] is also shown as Lorite-B (maximum base suction reduction around 6%). It represents base blowing being carried out from a horizontal slit spanning the bottom edge of the base. It is observed that the present fluid injection mechanism appears to be more energy efficient compared to base blowing carried out near the shear layers, as greater drag reduction is achieved along with lower  $C_q^{\text{opt}}$ .

Following the same idea as in Ref. [11], that the transition between the mass and the momentum regimes defining  $C_q^{\text{opt}}$  occurs when the injected momentum flux reaches a maximum value  $\Pi$  from

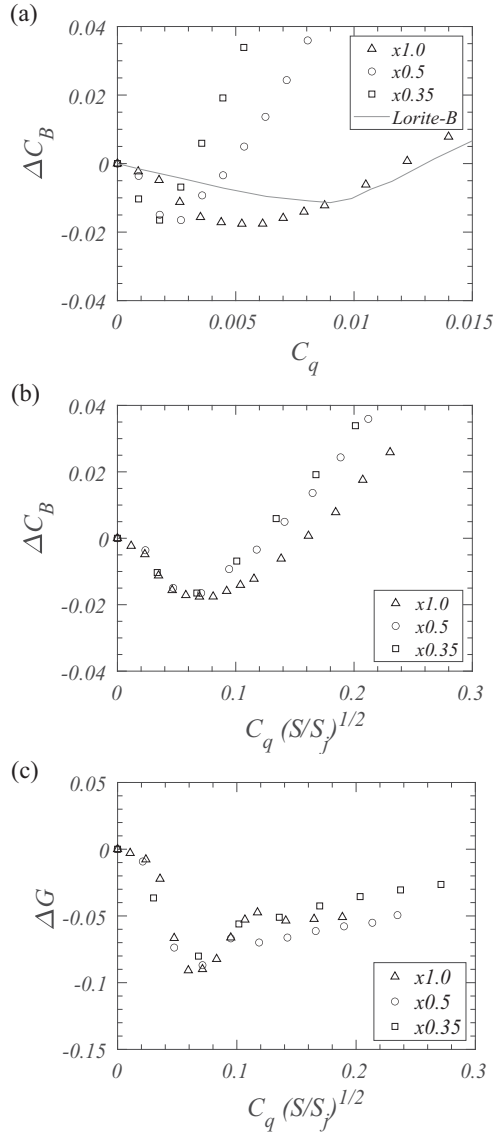


FIG. 4. Changes in base suction ( $\Delta C_B$ ) with respect to (a) the blowing coefficient  $C_q$  for all scales of steady jet actuator. Lorite-B results are from Ref. [11] (see text), and (b) the scaled coefficient as the power law of area ratio  $C_q(S/S_j)^{1/2}$ . (c) Changes in the wake asymmetry strength ( $\Delta G$ ) with respect to the scaled blowing coefficient  $C_q(S/S_j)^{1/2}$  for all three scales of the actuation jet.

which the mass injection cannot be considered as a passive scalar,

$$\Pi = \rho_j u_j^{\text{opt}} S_j u_j^{\text{opt}} = \frac{\rho_j}{S_j} (q_j^{\text{opt}})^2. \quad (5)$$

Equation (5) provides the scaling,

$$C_q^{\text{opt}} = b \sqrt{\frac{\rho}{\rho_j} \frac{S_j}{S}}, \quad (6)$$

where  $b^2 = \Pi/\rho U^2 s$  is the dimensionless maximum momentum flux bared by the bubble, consistent with the mass regime and  $\rho$  the density of the injected gas. In our case  $\rho/\rho_j = 1$  and Fig. 4(b) confirms satisfactorily the scaling (6) with  $b = 7.41 \times 10^{-2}$  for which all actuator scales collapse in the “mass” regime. The maximum injected momentum flux  $b^2 = 5.49 \times 10^{-3}$  cannot be compared to that reported in Ref. [11] ( $6.4 \times 10^{-5}$ ). There, a dilution factor had to be introduced in (5) in order to reproduce previous observation in Ref. [10] of a mass regime scaling with  $C_q$ , which is not the case here [see Fig. 4(a)].

The effects of the actuator jet scaling on the wake symmetry are shown in Fig. 4(c) with respect to the given scaling of the blowing coefficient. All three jet scales achieve a similar reduction in the wake asymmetry strength  $\Delta G = G - G_0$ . Furthermore, the  $C_q(S/S_j)^{1/2}$  scaling reveals this to occur for the same actuation regime at  $C_q^{\text{opt}}$ .

#### IV. CONCLUSIONS

To conclude, a centrally located base blowing using a steady jet is found to greatly suppress the steady wake asymmetry, which otherwise dominates the unactuated wake. A concurrent drag decrease of 6% is also recorded for the optimal blowing coefficient. A similar effect is also observed in the case of Refs. [23,25] when using a sweeping jet which is located centrally at the base, although the wake symmetrization does not correspond to a minimum drag, and the drag reduction is only around 3%. The square jet used in the current experiment has less entrainment and a lower spreading rate than a sweeping jet [26], and has no fixed frequency associated with it. These different dynamics plausibly account for the differences in the scaled blowing coefficients between the current experiment and results obtained by Ref. [25]. Furthermore, the scaling law coefficients differ from those observed in Ref. [11], indicating that both the blowing location and jet dynamics are the determining factors.

The proposed central blowing requires a lower mass flow rate of the actuator and provokes a greater drag reduction as compared to blowing from perimetric slits around the base [10,11]. Recent studies by Ref. [27] suggest a feedback mechanism of recirculating flow from one shear layer interacting and triggering vortex rollups in the opposing shear layer that leads to wake reversal. They also identified that a transient symmetric state during wake reversals correspond to a lower base drag. On the other hand, in the experiments involving the base cavity [21] and base suction [22] where the wake is symmetrized, results cannot be easily interpreted in the context of the proposed mechanism by Ref. [27]. In both cases, there is no strong actuation which can plausibly inhibit the interaction of the opposite shear layers. In the example of our current work, the jet at  $C_q^{\text{opt}}$  is quite weak and it is doubtful (although not impossible) that it can act as an inhibitor of the proposed interaction mechanism. Extensive flow field data would be necessary to further study the underlying mechanisms.

#### ACKNOWLEDGMENTS

This work has been supported by the Khalifa University of Science and Technology under Award No. CIRA-2019-025. The authors would also like to thank T. Pichon and L. Cherfa of the ENSTA-UME, and R. De Jesus and R. Ganithi of the KU Fabrication Laboratory, for their exceptional support in this experiment.

- 
- [1] C. J. Wood, The effect of base bleed on a periodic wake, *Aeronaut. J.* **68**, 477 (1964).
  - [2] P. W. Bearman, The effect of base bleed on the flow behind a two-dimensional model with a blunt trailing edge, *Aeronaut. Q.* **18**, 207 (1967).
  - [3] V. L. Zhdanov, Effect of jet bleed out of the base of a model on the base pressure and frequency characteristics of wake flow, *J. Eng. Phys. Thermophys.* **71**, 627 (1998).

- [4] J. L. F. Porteiro, C. E. G. Przirembel, and R. H. Page, Modification of subsonic wakes using boundary layer and base mass transfer, *AIAA J.* **21**, 665 (1983).
- [5] G. K. Suryanarayana and G. E. A. Meier, Effect of ventilation on the flowfield around a sphere, *Exp. Fluids* **19**, 78 (1995).
- [6] A. Sevilla and C. Martínez-Bazán, Vortex shedding in high Reynolds number axisymmetric bluff-body wakes: Local linear instability and global bleed control, *Phys. Fluids* **16**, 3460 (2004).
- [7] A. R. Oxlade, J. F. Morrison, A. Qubain, and G. Rigas, High-frequency forcing of a turbulent axisymmetric wake, *J. Fluid Mech.* **770**, 305 (2015).
- [8] J. M. Garcia de la Cruz, A. R. Oxlade, and J. F. Morrison, Passive control of base pressure on an axisymmetric blunt body using a perimetric slit, *Phys. Rev. Fluids* **2**, 043905 (2017).
- [9] R. P. Littlewood and M. A. Passmore, Aerodynamic drag reduction of a simplified squareback vehicle using steady blowing, *Exp. Fluids* **53**, 519 (2012).
- [10] M. Lorite-Díez, J. Jiménez-González, L. Pastur, C. Martínez-Bazán, and O. Cadot, Experimental analysis of the effect of local base blowing on three-dimensional wake modes, *J. Fluid Mech.* **883**, A53 (2020).
- [11] M. Lorite-Díez, J. Jiménez-González, L. Pastur, O. Cadot, and C. Martínez-Bazán, Drag reduction of three-dimensional bodies by base blowing with various gas densities, *Phys. Rev. E* **102**, 011101 (2020).
- [12] J. Howell, D. Sims-Williams, A. Sprot, F. Hamlin, and R. Dominy, Bluff body drag reduction with ventilated base cavities, *SAE Int. J. Passeng. Cars - Mech. Syst.* **5**, 152 (2012).
- [13] Y. I. Brown, S. Windsor, and A. Gaylard, The effect of base bleed and rear cavities on the drag of an SUV, in *SAE Technical Paper Series* (SAE International, Detroit, Michigan, United States of America, 2010).
- [14] M. Grandemange, M. Gohlke, and O. Cadot, Turbulent wake past a three-dimensional blunt body. Part 1. Global modes and bi-stability, *J. Fluid Mech.* **722**, 51 (2013).
- [15] O. Cadot, A. Evrard, and L. Pastur, Imperfect supercritical bifurcation in a three-dimensional turbulent wake, *Phys. Rev. E* **91**, 063005 (2015).
- [16] M. Grandemange, M. Gohlke, and O. Cadot, Turbulent wake past a three-dimensional blunt body. Part 2. Experimental sensitivity analysis, *J. Fluid Mech.* **752**, 439 (2014).
- [17] M. Grandemange, O. Cadot, A. Courbois, V. Herbert, D. Ricot, T. Ruiz, and R. Vigneron, A study of wake effects on the drag of Ahmed's squareback model at the industrial scale, *J. Wind Eng. Ind. Aerodyn.* **145**, 282 (2015).
- [18] D. Barros, J. Borée, O. Cadot, A. Spohn, and B. R. Noack, Forcing symmetry exchanges and flow reversals in turbulent wakes, *J. Fluid Mech.* **829**, R1 (2017).
- [19] Y. Haffner, T. Castelain, J. Borée, and A. Spohn, Manipulation of three-dimensional asymmetries of a turbulent wake for drag reduction, *J. Fluid Mech.* **912**, A6 (2021).
- [20] D. Bao, J. Borée, Y. Haffner, and C. Sicot, Near wake interactions and drag increase regimes for a square-back bluff body, *J. Fluid Mech.* **936**, A2 (2022).
- [21] A. Evrard, O. Cadot, V. Herbert, D. Ricot, R. Vigneron, and J. Délerly, Fluid force and symmetry breaking modes of a 3D bluff body with a base cavity, *J. Fluids Struct.* **61**, 99 (2016).
- [22] E.-C. Hsu, L. Pastur, O. Cadot, and V. Parezanović, A fundamental link between steady asymmetry and separation length in the wake of a 3D square-back body, *Exp. Fluids* **62**, 95 (2021).
- [23] D. Veerasamy, A. R. Tajik, L. Pastur, and V. Parezanović, Effect of base blowing by a large-scale fluidic oscillator on the bistable wake behind a flat-back Ahmed body, *Phys. Fluids* **34**, 035115 (2022).
- [24] J. H. Gerrard, The mechanics of the formation region of vortices behind bluff bodies, *J. Fluid Mech.* **25**, 401 (1966).
- [25] T. I. Khan, A. R. Tajik, and V. Parezanović, Drag reduction of a generic transport vehicle model using a fluidic oscillator, *Int. J. Thermofluids* **15**, 100180 (2022).
- [26] F. Ostermann, R. Woszidlo, C. N. Nayeri, and C. O. Paschereit, Properties of a sweeping jet emitted from a fluidic oscillator, *J. Fluid Mech.* **857**, 216 (2018).
- [27] Y. Haffner, J. Borée, A. Spohn, and T. Castelain, Mechanics of bluff body drag reduction during transient near-wake reversals, *J. Fluid Mech.* **894**, A14 (2020).